Journal of Materials Chemistry A

Accepted Manuscript

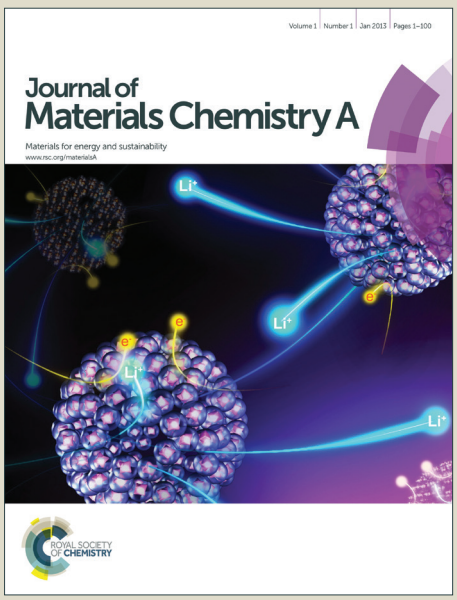

ROYAL SOCIETY OF CHEMISTRY

www.rsc.org/materialsA

Journal Name

RSCPublishing

ARTICLE

The Effect of Carbon Counter Electrode on Fully Printable Mesoscopic Perovskite Solar Cell

Cite this: DOI: 10.1039/x0xx00000x

Lijun Zhang, Tongfa Liu, Linfeng Liu, Min Hu, Ying Yang, Anyi Mei, Hongwei Han*

Received ooth January 2012,
Accepted ooth January 2012

DOI: 10.1039/x0xx00000x

www.rsc.org/

Mesoporous graphite/carbon black counter electrodes (CEs) using flaky graphite with different sizes were applied in hole-conductor-free mesoscopic perovskite solar cells by screen-printing technique. Conductivity measurements, current-voltage characteristics, and impedance spectroscopy measurements were carried out to study the influence of CEs on the photovoltaic performance of devices. The results indicated that graphite, which acted as the conductor in carbon counter electrodes (CCEs), could significantly affect the square resistance of CCEs, thus resulting in differences in fill factor and power conversion efficiency (PCE) of the devices. Based on the optimized CCE with a thickness of 9 μm, PCEs exceeding 11% could be achieved for the fully printable hole-conductor-free mesoscopic perovskite solar cells due to the low square resistance and large pore size of graphite based CCEs. The abundant availability, low cost and excellent properties of such carbon materials based CEs offer a wide prospect for its further applications in perovskite solar cells.

Introduction

Since the initial report from T. Miyasaka group on applying $CH_3NH_3PbBr_3$ as the light harvester in a liquid-state perovskite-sensitized solar cell with a power conversion efficiency (PCE) of 3.8%,[1] organometal halide perovskite has attracted considerable attention due to its direct band gap, high absorption coefficient, and high carrier mobility.[2-4] To solve the problem that the perovskite material would dissolve in the liquid-state electrolyte, solid-state hole-transporting-materials (HTMs) such as Spiro-OMeTAD were employed as hole conductors to assemble perovskite solar cells.[5] Up to now, the certified power conversion efficiency of mesoscopic perovskite solar cells has increased to over 16%[6-10], which makes it a promising candidate of the next generation photovoltaic technology. However, compared with other components in such devices, the existence of HTMs and noble metal (such as Au or Pt) based counter electrodes bear a large proportion of the material cost,[11, 12] limiting their approach to low-cost photovoltaic devices. Furthermore, the vacuum evaporation process of noble metal electrodes is highly energy consumptive, which would block the large-scale production of the devices.

Therefore, it is worth developing hole-conductor-free mesoscopic perovskite solar cells and replacing the noble-metal-based CEs with inexpensive and abundantly available materials. Previously, we have reported the fully printable mesoscopic perovskite solar cells with carbon counter electrodes (CCEs). Employing a simple drop-coating method to infiltrate the perovskite $CH_3NH_3PbI_3$ into the TiO_2/ZrO_2/Carbon layers, the device without a HTM layer showed a PCE of 6.64%[13]. Then, we used TiO_2 nanosheets instead of TiO_2 nanoparticles as the electron collector, and obtained a PCE of 10.64% for the hole-conductor free mesoscopic perovskite solar cells based on CCEs[14]. Also a device with high stability and a certified efficiency of 12.84% has recently been reported in our group[15]. Compared with Au or Pt CEs, printable CCEs are much cheaper and easier to process, especially for large-scale production. Thus, using CCEs in mesoscopic perovskite solar cells will simultaneously cut both material costs and production costs, offering a more encouraging prospect for the commercialization of this photovoltaic technology. Generally, the CCEs employed graphite and carbon black as the main components, and presented a mesoporous structure. Although many valuable studies have suggested that carbon can be a promising candidate for perovskite solar cells, relevant reports on employing CCEs in perovskite solar cells remain scarce.

Herein, we studied the impact of the graphite's size in the graphite/carbon black CEs on the photovoltaic performance of hole-conductor-free mesoscopic perovskite solar cells. The work function, homogeneity, average pore size and the square resistance of CCEs have been measured and investigated. For the devices, current-voltage characteristics and IS measurements were carried out to analyze the influence of the CCEs on the device performance. As a result, an optimal

efficiency of 11.65% was obtained under AM 1.5 illumination of 1000 W/m^2.

Experimental

Fabrication of graphite/carbon black paste. Carbon paste was prepared as reported previously.[16, 17] 2 g carbon black powders (particle size: 30 nm) mixed with 6 g graphite powders in a 30 mL terpineol solution, and then 1 g of 20 nm ZrO_2 nanopowders and 1 g of hydroxypropyl cellulose were added into solution, followed by stirring vigorously using ball milling for 2 h.

Fabrication of hole-conductor-free mesoscopic perovskite solar cells. FTO glass was etched with a laser to form two detached electrode pattern before being ultrasonically cleaned with detergent, deionized water and ethanol successively. Then, the substrates were coated with a compact TiO_2 by aerosol spray pyrolysis at 450 ˚C for 30 min. After that, a 400 nm TiO_2 nanocrystalline layer was deposited on the top of the compact layer by screen-printing technology and then sintered at 500˚C for 30 min. After cooling to room temperature, a 500 nm ZrO_2 nanocrystalline layer and a 9 μm mesoscopic carbon layer were printed successively, which were sintered at 400 ˚C for 30 min. Finally, 1.5 μL saturated PbI_2 precursor was dipped through the mesoscopic carbon layer, followed by drying at 70˚C for 30 min on the hot plate, then the cells were dipped into a methylammonium iodide 2-propanol solution for 12 min. The resulting perovskite films were black in color, seen from the anode side after drying at 70˚C for 30 min, demonstrating the completion of the fabrication of devices.

Characterization. The cross section of graphite powder and the CCE were imaged by a field-emission scanning electron microscope (FE-SEM). The four-probe tests were carried out on the CCE of 8 cm × 16 cm for their conductivity measurement. The photocurrent density-voltage characteristics were taken with a Keithley 2400 sourcemeter under illumination with an Oriel solar simulator composed of a 1000 W Xenon arc lamp and AM 1.5 G filters. Light intensity was calibrated with a normative silicon cell. The impedance spectroscopy (IS) of the devices was characterized using a potentiostat (EG&G, M2273) with the measured frequency range from 1 MHz to 10 mHz under the same illumination. The Brunauer-Emmett-Teller (BET) was characterized by ASAP 2020 accelerated surface area and porosimetry system. The normalized incident-photon-to-electron conversion efficiencies (IPCE) were measured using a 150 W xenon lamp (Oriel) fitted with a monochromator (Cornerstone 74004) as a monochromatic light source.

Results and Discussion

Structure of fully printable hole-conductor-free mesoscopic perovskite solar cells. For hole-conductor-free mesoscopic perovskite solar cells, the perovskite layer can act as both a light absorber and a hole conductor, rendering superfluous the use of an additional p-type material for transporting positive charge carries and also simplifying the structure of devices greatly. **Fig. 1a)** presents a scheme of the device structure. The whole device is composed of a hole-blocking compact TiO_2 layer deposited on a FTO glass substrate by aerosol spray pyrolysis, followed by screen-printing a 400 nm thick layer of TiO_2 nano-particle paste, a 500 nm thick layer of ZrO_2 and a 9 μm thick layer of carbon, confirmed by the scanning electron microscope (SEM) image in **Fig 1c)**. After dropping 1.5 μL PbI_2 precursors from the mesoscopic CCEs side followed by sintering at 70 °C for 30 min, the samples were dipped into the methylammonium iodide 2-propanol solution for 12 min, and then finished with another identical sinter process. Observed from the anode side, the absorber layer darkened in color, indicating the formation of $CH_3NH_3PbI_3$ is in the solid state.

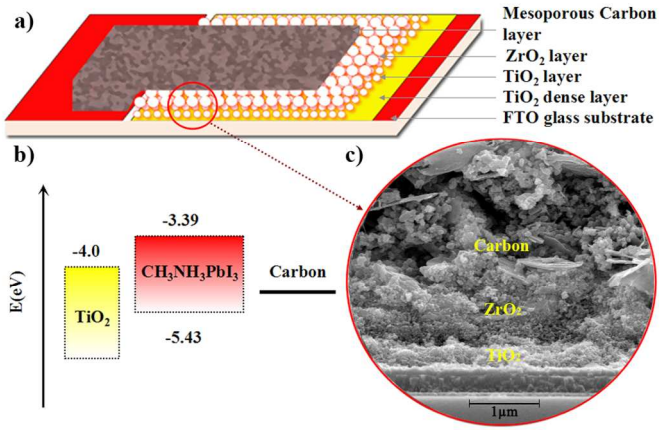

Fig. 1 a) The schematic structure of a CCE based perovskite solar cells. **b)** The corresponding energy levels of TiO_2, $CH_3NH_3PbI_3$ and Carbon. **c)** A SEM image of the devices.

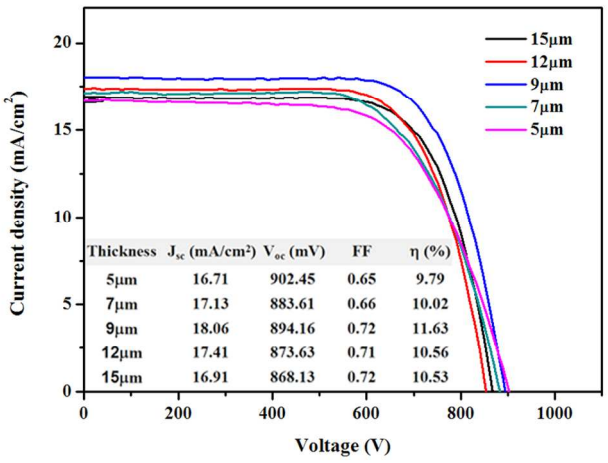

Thickness	J_{sc} (mA/cm²)	V_{oc} (mV)	FF	η (%)
5μm	16.71	902.45	0.65	9.79
7μm	17.13	883.61	0.66	10.02
9μm	18.06	894.16	0.72	11.63
12μm	17.41	873.63	0.71	10.56
15μm	16.91	868.13	0.72	10.53

Fig. 2 Photocurrent density-voltage (*J-V*) curves of devices based on CCEs with different thicknesses. Inset shows the detailed parameters of *J-V* curves.

Studies have rarely reported on that the CEs, as an essential part of mesoscopic perovskite solar cells, actually have significant influences on the device performance, especially for the mesoporous CCEs based perovskite solar cells[14-17]. Theoretically, the thickness of mesoporous CCEs will affects the crystallization of PbI_2 and $CH_3NH_3PbI_3$ significantly, since

it is the pathway for the infiltration of both PbI_2 and CH_3NH_3I precursors. An over-thick layer of CCEs will restrict the diffusion of the PbI_2 precursor from the CCE layer to the TiO_2 layer, resulting in incomplete pore filling, while an over-thin CCE will decrease the FF of the device owing to the lack of conductivity. Therefore, the thickness of the CCEs should be optimized.

In order to understand the exact effect of mesoscopic CCEs and obtain the optimal thickness, a series of devices have been fabricated in this work. **Fig. 2** presents photocurrent density-voltage characteristics of these devices under AM 1.5 illumination of 1000 W/m^2, and detailed parameters were summarized in the inset. It could be found that the maximal performance of the devices is obtained when the thickness of the carbon layer is *ca.* 9 μm. The device presents a V_{oc} of 894 mV, a J_{sc} of 18.06 mA/cm^2, and a FF of 0.72, corresponding to a PCE of 11.63%. Compared with 9 μm thick CCE based devices, the declines in J_{sc} caused by incomplete pore filling of PbI_2 eventually decrease the PCE of devices. On the other hand, for over-thin CCE based devices, the huge decrease of FF induced by large square resistance results in a sharp decrease in efficiency. Therefore, the thickness of CCEs was optimized to *ca.* 9 μm.

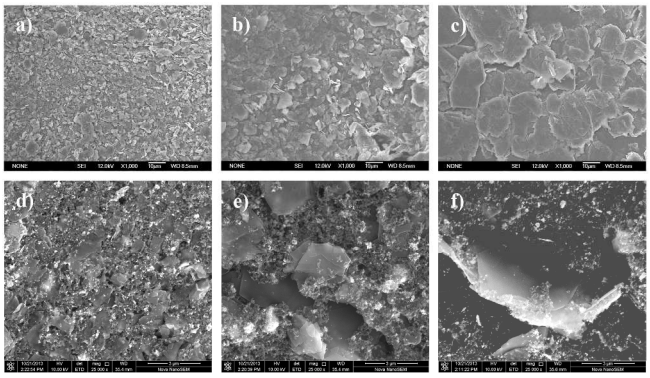

Fig. 3a-c) SEM images of graphite powder with different particle sizes, which is *ca.* 500 nm, 3 μm, 8 μm, respectively. **d-f)** Top-view images of CCEs using graphite with different sizes.

Table 1 0.2~0.4 g powder of CCEs using graphite of different sizes have been used for BET test. Square resistance were derived from 9 μm thick CCEs with area of 8 mm × 16 mm.

Size	BET (m^2g^{-1})	Average pore (nm)	R_{sq} (Ω)
500 nm	127.83	12.177	56.68
3 μm	140.08	10.765	132.26
8 μm	111.09	15.030	11.47

Table 2 Square resistance of 9 μm thick CCEs employing graphite with different sizes.

	8 μm	6 μm	3 μm	500 nm	40 nm
R_{sq} (Ω)	11.47	61.21	132.26	56.68	63.01

Characterization of CCEs with different sized graphite. The SEM images of CCEs with different sized graphite are presented in **Fig. 3a-c)**. The diameters of the graphite are *ca.* 500 nm, 3 μm and 8 μm in Fig. 3a to 3c, respectively. The CCE paste was prepared by mixing aforementioned graphite with carbon black and ZrO_2. **Fig. 3d-f)** presents the top view of the mesoscopic carbon layer fabricated by screen-printing technique, and it is easy to observe that both ZrO_2 and carbon black powders were homogeneously dispersed. After sintering at 400 °C for 30 min, the Brunauer-Emmett-Teller (BET) test shows that 8 μm graphite based CCEs achieved the biggest average pore size, *ca.* 15 nm (as shown in **Table 1**), which means that it should be easier for the filling of precursors, corresponding with the diffusion rate of PbI_2 precursor on CCEs observed in practice. **Table 1** also presents the square resistance of CCEs with different sized graphite. The square resistance of 8 μm graphite based CCEs are more than 10 times bigger than 3 μm ones, indicating that the size of graphite has a significant influence on conductivity of CCEs. In order to be thorough, we intentionally extend the size of graphite ranges from 40 nm to 8 μm. As shown in **Table 2**, the square resistance of CCE layers with the thickness of 9 μm, tested by the four-probe method, clearly increases with an increase in the size of graphite above 1 μm. It is easy to understand that a lower breaking point between flaky graphite with the same quality will lead to a lower square resistance. Following this trend, the square resistance of 500 nm graphite based CCE is supposed to be larger, but it is actually quite close to the micro-range graphite. We speculate that 500 nm graphite based CCEs contain much more graphite, which is more than enough to induce the huge difference in conductivity compared with micro-range graphite based CCEs of the same volume, that results in the low square resistance.

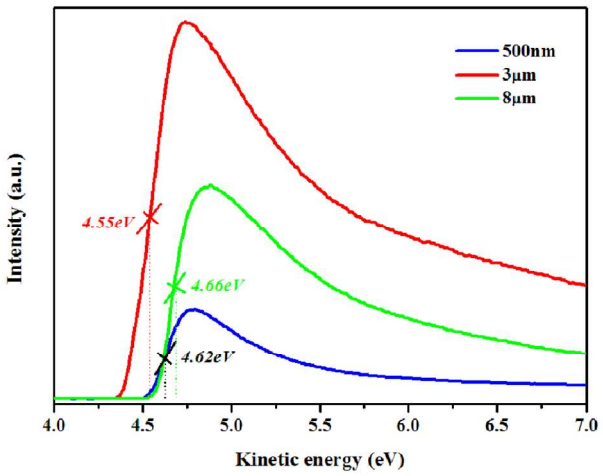

Fig. 4 X-ray photoelectron spectroscopy (XPS) test of CCEs using graphite of different sizes.

It is well known that Energy level matching between the perovskite and CE will be vital to whether the device can function well or not. The energy band diagram of the devices is sketched in **Fig. 1b)**. The conduction and valence bands of the $CH_3NH_3PbI_3$ permit electron injection into TiO_2 and hole transport to the CCE, respectively. **Fig. 4** presents the work function of CCEs using graphite of different sizes, achieved by

X-ray photoelectron spectroscopy (XPS) test. It could be found that the difference between these three kinds of CCEs is about 0.1 eV, which is within the experimental errors compared with the work function of CCEs. Therefore, we may deduce that the difference in the energy bandgap may not be obvious enough to distinguish the V_{oc} of devices based on CCEs using these different sized graphites during the actual experiment progress.

Characterization of devices based on CCEs with different sized graphite. IS measurement is regarded as a useful technology to provide abundant and crucial information on the working mechanism of each part of all kinds of photovoltaic devices[18, 19], such as liquid dye-sensitized solar cells (DSCs) and all-solid-state DSCs[20, 21]. And it is also beginning to be used in the characterization of perovskite solar cells. Theoretical studies of perovskite solar cells remained undeveloped until the report from M. Grätzel on impedance spectroscopic analysis of lead-iodide perovskite-sensitized solid-state solar cells[22], whose device structure is almost the same as ours, except for the absence of HTMs. Most recently, Ivan and his coworkers reported on the role of the selective contacts in the performance of lead halide perovskite solar cells[23]. Based on Ivan's model, the impedance spectroscopic analysis of HTM-free solar cells can be more valid.

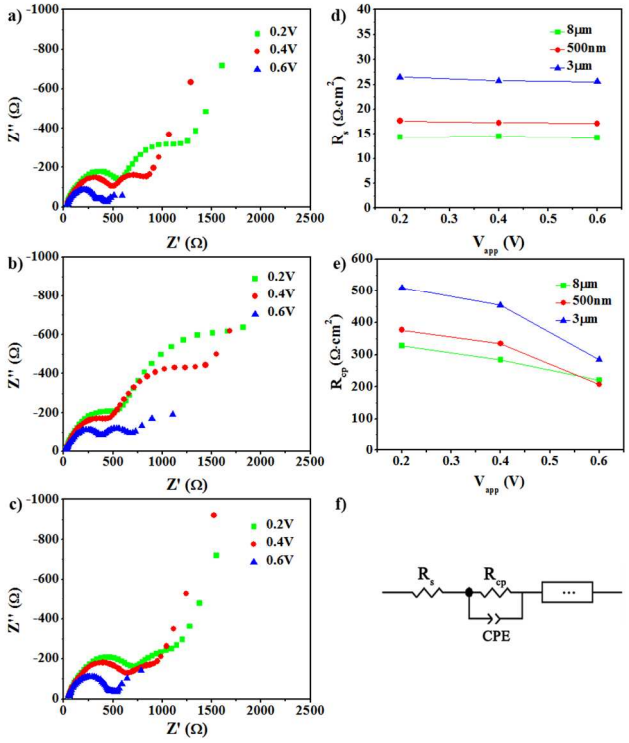

Fig. 5 a-c) Nyquist plots of devices based on CCEs with graphite of different sizes. **d-e)** R_s and R_{cp} extracted from Nyquist plots *vs.* potential. **f)** Equivalent circuit being used to fit the Nyquist curves.

Fig. 5a-c) depicts the IS images of solar cells under the same illumination at different potential. The equivalent circuit is shown in figure **Fig. 5f)**. In this paper, we only focus on the discussion of series resistance (R_s) and charge transform resistance between CCEs and perovskite (R_{cp}) in consideration of relevance to the CCEs. **Fig. 5d-e)** shows the parameters extracted from IS images. According to the results, R_s are scarcely changed under different potentials for all these three kinds of devices, as shown in **Fig. 5d),** and also the value of R_s is consistent with the trend of square resistances of CCEs shown in **Table 1**. That is to say, graphite applied in CCEs have a non-trivial effect on R_s. R_{cp} is the resistance associated with the high-frequency feature in Nyquist plots. As we know, R_s and R_{cp} were an important part of total series resistance of the devices. Consequently, low values are preferable. So according to **Fig. 5d-e)**, devices applying 8 μm graphite based CCEs should have a better performance due to their lower value of total series resistance.

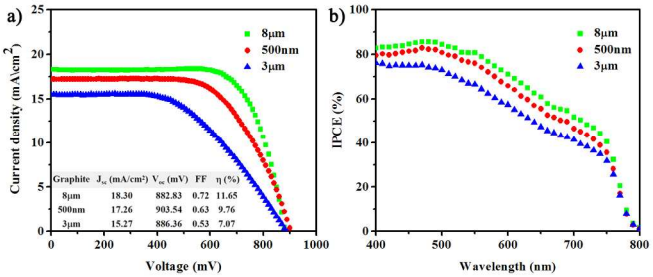

Fig. 6 a) Photocurrent density-voltage (*J-V*) curves of devices based on CCEs with different sizes graphite, which is 8 μm (green points), 500 nm (red points), and 3 μm (blue points), respectively. Inset shows the detail parameters of Current-voltage curves. **b)** IPCE measured under a 150 W xenon lamp.

It is well known that the series resistance of CEs will influence the FF parameter[16, 23], which determines the shape of current-voltage characteristics and the maximum power output of the device. **Fig. 6a)** presents the photocurrent density-voltage characteristics of our devices under standard simulated AM 1.5 illumination of 1000 W/m^2. The photovoltaic parameters are summarized in the inset, which shows that the best performance achieved with the device employs 8 μm graphite based CCEs and presents V_{oc} of 882 mV, J_{sc} of 18.30 mA/cm^2 and *FF* of 0.72, corresponding to a PCE of 11.65%. Apparently, it could be found that the main difference of the devices based on CCEs with different sized graphite is in *FF*, eventually leading to the difference on PCE. As expected previously, 8 μm graphite based solar cells achieved the biggest FF of 0.72 compared with the 500 nm and 3 μm ones, which is 0.63 and 0.53 respectively, in reasonable agreement with the trend of R_s and R_{cp}. And also the incident photon-to-electron conversion efficiency (IPCE) spectrum (**Fig. 6b)**) is plotted as a function of wavelength of the incident light, confirming the difference in J_{sc}. Under a 150 W xenon lamp, the device with the best performance shows an excellent photocurrent response from 400 to 800 nm, with the IPCE reaching a maximum of more than 80% in the wavelength range of 400-500 nm and decreasing at longer wavelengths until 800 nm.

Conclusions

In summary, as a key component, graphite has a huge influence on the porosity and conductivity of CCEs. Changes in the size of graphite will induce differences in the filling of PbI_2 and

$CH_3NH_3PbI_3$ precursors and also the square resistance of CCEs, which will eventually result in the difference in PCE of devices. A series of devices have been made to study the exact impact of graphite, which indicated that the 8 μm graphite based CCEs generally got a larger average pore size, a smaller square resistance and hence a higher PCE exceeding 11% compared with others. The fully printable hole-conductor-free mesoscopic perovskite solar cells based on CCEs have the potential to realize large-scale fabrication in the near future.

Acknowledgements

The authors acknowledge the financial support from the Ministry of Science and Technology of China (863, No. SS2013AA50303), the National Natural Science Foundation of China (Grant No. 61106056), the Science and Technology Department of Hubei Province (No. 2013BAA090) and the Fundamental Research Funds for the Central Universities (HUSTNY022). We thank the Analytical and Testing Center of Huazhong University of Science and Technology (HUST) for field emission scanning electron microscopy (FE-SEM) testing.

Notes and references

Michael Grätzel Center for Mesoscopic Solar cells, Wuhan National Laboratory for Optoelectronics. School of Optical and Electronic Information, Huazhong University of Science and Technology, Wuhan, Hubei, P. R. China, 430074. E-mail: hongwei.han@mail.hust.edu.cn; Tel: +86 27 8779 3027

1. A. Kojima, K. Teshima, Y. Shirai and T. Miyasaka, *J Am Chem Soc*, 2009, **131**, 6050-6051.
2. L. Etgar, P. Gao, Z. Xue, Q. Peng, A. K. Chandiran, B. Liu, M. K. Nazeeruddin and M. Grätzel, *J Am Chem Soc*, 2012, **134**, 17396-17399.
3. A. Kojima, M. Ikegami, K. Teshima and T. Miyasaka, *Chem Lett*, 2012, **41**, 397-399.
4. C. R. Kagan, D. B. Mitzi and C. D. Dimitrakopoulos, *Science*, 1999, **286**, 945-947.
5. H.-S. Kim, C.-R. Lee, J.-H. Im, K.-B. Lee, T. Moehl, A. Marchioro, S.-J. Moon, R. Humphry-Baker, J.-H. Yum, J. E. Moser, M. Grätzel and N.-G. Park, *Scientific Reports*, 2012, **2**.
6. N. J. Jeon, H. G. Lee, Y. C. Kim, J. Seo, J. H. Noh, J. Lee and S. I. Seok, *J Am Chem Soc*, 2014, **136**, 7837-7840.
7. N. J. Jeon, J. H. Noh, Y. C. Kim, W. S. Yang, S. Ryu and S. I. Seok, *Nature Materials*, 2014.
8. S. Ryu, J. H. Noh, N. J. Jeon, Y. Chan Kim, W. S. Yang, J. Seo and S. I. Seok, *Energy & Environmental Science*, 2014, **7**, 2614-2618.
9. M. A.Green, K. Emery, Y. Hishikawa, W. Warta, E. D. Dunlop, *Prog. Photovolt. Res. Appl.* 2014, **22**, 701-710.
10. B. Wang, X. Xiao, and T. Chen, *Nanoscale,* 2014.
11. J. Burschka, N. Pellet, S.-J. Moon, R. Humphry-Baker, P. Gao, M. K. Nazeeruddin and M. Grätzel, *Nature*, 2013, **499**, 316-319.
12. J. H. Heo, S. H. Im, J. H. Noh, T. N. Mandal, C.-S. Lim, J. A. Chang, Y. H. Lee, H.-j. Kim, A. Sarkar, K. NazeeruddinMd, M. Gratzel and S. I. Seok, *Nat Photon*, 2013, **7**, 486-491.
13. Z. Ku, Y. Rong, M. Xu, T. Liu and H. Han, *Sci. Rep.*, 2013, **3**.
14. Y. Rong, Z. Ku, A. Mei, T. Liu, M. Xu, S. Ko, X. Li and H. Han, *The Journal of Physical Chemistry Letters*, 2014, **5**, 2160-2164.
15. A. Mei, X. Li, L. Liu, Z. Ku, T. Liu, Y. Rong, M. Xu, M. Hu, J. Chen, Y. Yang, M. Grätzel and H. Han, *Science*, 2014, **345**, 295-298.
16. G. Liu, H. Wang, X. Li, Y. Rong, Z. Ku, M. Xu, L. Liu, M. Hu, Y. Yang, P. Xiang, T. Shu and H. Han, *Electrochimica Acta,* 2012, **69**, 334-339.
17. M. Xu, G. Liu, X. Li, H. Wang, Y. Rong, Z. Ku, M. Hu, Y. Yang, L. Liu, T. Liu, J. Chen and H. Han, *Organic Electronics,* 2013, **14**, 628-634.
18. F. Fabregat-Santiago, G. Garcia-Belmonte, I. Mora-Sero and J. Bisquert, *Phys Chem Chem Phys*, 2011, **13**, 9083-9118.
19. I. Mora-Sero, G. Garcia-Belmonte, P. P. Boix, M. A. Vazquez and J. Bisquert, *Energy & Environmental Science*, 2009, **2**, 678-686.
20. P. P. Boix, G. Larramona, A. Jacob, B. Delatouche, I. Mora-Seró and J. Bisquert, *The Journal of Physical Chemistry C*, 2011, **116**, 1579-1587.
21. P. P. Boix, Y. H. Lee, F. Fabregat-Santiago, S. H. Im, I. Mora-Sero, J. Bisquert and S. I. Seok, *Acs Nano*, 2011, **6**, 873-880.
22. A. Dualeh, T. Moehl, N. Tétreault, J. Teuscher, P. Gao, M. K. Nazeeruddin and M. Grätzel, *Acs Nano*, 2013, **8**, 362-373.
23. E. J. Juarez-Perez, M. Wuβler, F. Fabregat-Santiago, K. Lakus-Wollny, E. Mankel, T. Mayer, W. Jaegermann and I. Mora-Sero, *The Journal of Physical Chemistry Letters*, 2014, **5**, 680-685.

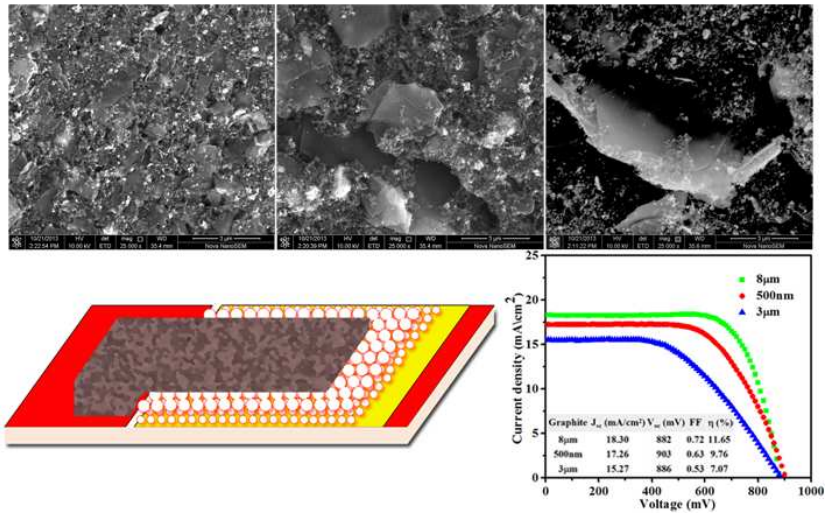

The size effect of graphite on hole-conductor-free fully printable mesoscopic perovskite solar cell was studied.